Journal of Cluster Science
https://doi.org/10.1007/s10876-022-02330-6

ORIGINAL PAPER

Synthesis of Cu_2S Ultrasmall Nanoparticles in Zeolite 4A Nanoreactor

J. E. Leal-Perez[1] · J. Flores-Valenzuela[1] · R. A. Vargas-Ortíz[1] · C. G. Alvarado-Beltrán[1] · A. Hurtado-Macias[2] · J. L. Almaral-Sánchez[1]

Received: 8 May 2022 / Accepted: 6 July 2022

Abstract
In this work, Cu_2S ultrasmall nanoparticles were synthesized in a zeolite 4A nanoreactor (ZA) by the ion exchange method, which consisted of two steps: (1) the ion exchange of Na^+, located in ZA, for Cu^+ and Cu^{2+}, and (2), formation of Cu_2S nanoparticles, using Na_2S by metathesis reaction (double displacement reaction). The molecular structure of ZA was verified by FT-IR and XRD and the formation of Cu_2S nanoparticles in the ZA matrix by DSC, UV–Vis, Raman, TEM, and HRTEM characterizations. The results showed a non-modified molecular structure of the Z4 by synthesis of Cu_2S nanoparticles with a size distribution of 4–8 nm.

Keywords Cu_2S nanoparticles · Zeolite 4A · Nanoreactor · Copper sulfide · Chalcocite

Introduction

Nanoreactors are small-sized chemical reactors where chemical reactions can be controlled and carried out [1]. And they have the ability to create a unique chemical environment that is different from the surrounding space as it can isolate the compounds from the outside mass and affect the reaction inside the nanoreactor [2]. Zeolite nanoreactor is used to promote uniform nanoparticle formation and inhibit the sintering of active nanoparticles [3].

Zeolites have attracted the attention of scientists since they were discovered in nature, because of their excellent physicochemical properties, especially in catalysis and adsorption-separation [4]. The zeolites are hydrated crystalline aluminosilicates with a uniform microporous structure formed by cages and channels with a molecular dimension of 2.5–12 A in size, making them suitable to accommodate sub-nanometer particles and clusters. In addition, their high surface area and excellent ion-exchange properties make interesting functional materials [5, 6]. Zeolite A has a cavity with a minimum free diameter of 1.14 nm, which may allow the growth of larger nanoparticles in it [7]. On the other hand, the use of different acidic or alkaline substances may cause mesoporous of size 5–50 nm. [8, 9]. Recently, zeolites have been used as hosts or templates to synthesize new nanomaterials, which have a great interest because of their unique and promising properties. In this route, Ag, Pd, and Cu-based nanoparticles and clusters have been synthesized within the zeolite pores, resulting in confined [10, 11], encapsulated [12], or just supported nanoparticles [13]. The nanoparticles inside the zeolites can have different types of applications [14–16]. In the case of nanoparticles of copper sulfide, could be an electrocatalyst application [17].

The semiconductors nanoparticles are one of the most exciting materials in recent years, and it is considered for the future due to their advanced and novel ways of applications [18]. Some semiconductors have been hosted in zeolites, such as nanoparticles of nickel sulfide (NiS), and cobalt sulfide (CoS) with sizes 6–10 nm, in mordenite zeolite [19, 20]. In addition, nanocluster of gallium sulfide (Ga_2S_3) in zeolite Y [21], cadmium sulfide (CdS) in A4 and MCM [22, 23], ETS [24] and Y [25] are also reported. Considering the chalcogenides, the copper sulfide compounds have been attractive and are receiving substantial attention for many applications because there are not toxic and have excellent photo and physicochemical properties [26].

✉ J. L. Almaral-Sánchez
jalmaral@uas.edu.mx

[1] Universidad Autónoma de Sinaloa, Fuente de Poseidón y Prol. Ángel Flores S/N, Fracc. Las Fuentes, Los Mochis, Sinaloa 81223, México

[2] Department of Metallurgy and Structural Integrity, National Nanotechnology Laboratory, Centro de Investigación en Materiales Avanzados, S.C., S. C. Miguel de Cervantes #120, Complejo Industrial Chihuahua, Chihuahua, Chihuahua 31136, México

Published online: 02 August 2022

The understanding of Copper sulfide properties and their many possible stoichiometries ($Cu_{2-x}S$) and crystal phases such as chalcocite (Cu_2S, monoclinic/hexagonal), djurleite ($Cu_{1.9}5S$, monoclinic), digenite ($Cu_{1.8}S$, cubic), anilite ($Cu_{1.75}S$, orthorhombic), and covellite (CuS, hexagonal) are still lacking [27, 28]. Covellite and chalcocite synthesized as nanostructures are the most studied copper sulfides due to their absorption bandgap in the near-infrared region [29, 30]. They have been reported in zeolites; for instance, CuS nanoparticles of 125 nm average size with spherical morphology in zeolitic imidazole framework-8 were encapsulated without affecting its crystal structure [31].

Only was found one work of Cu_2S nanoparticles of 32 nm on size average synthetized in RWY zeolite by the ion exchange method, which resulted in complex with multiples steps, and it did not allow the Cs^+ ions to be exchanged completely, furthermore, the structure of the zeolite can be destroyed for higher concentrations the Cu^{2+} solution [17]. In this work, we report the synthesis of Cu_2S ultrasmall nanoparticles in zeolite A4 nanoreactor by ion-exchange, performing a simple two-step process as an alternative to contribute to the continuous development of accessible and green strategies to synthesize copper sulfides nanostructures in zeolites. With this procedure and using zeolite as a nanoreactor, the nanoparticles obtained were four times smaller and more uniform in size than those reported in the literature. The Cu_2S nanoparticles were successfully synthesized in ZA and have been characterized by DRX, FTIR, UV–Vis, DSC, Raman, and TEM. The particle size, less than 10 nm, and the Cu_2S structures were identified by indexing the crystal plane by HR-TEM, which is the most used for the identification of nanoparticles [15, 23, 32–34].

Materials and Methods

Materials

Synthetic zeolite 4A (ZA, Sigma-Aldrich), cupric sulfate ($Cu_2SO_4.5H_2O$, 99.5%, Faga Lab), Sodium sulfide ($Na_2S.9H_2O$, 98%, Faga Lab), deionized water, Faga Lab.

Method

The experimental method used, applied in previous work [35], consists of two steps, as follows.

Step 1: Cu Ion Exchange in ZA (ZACu)

First, 10 g of ZA was dissolved in 50 ml of deionized water for 12 h for its hydration. At the same time, a solution of 150 ml of $CuSO_4$ (0.1 M) was prepared. Next, the $CuSO_4$ solution and the hydrated ZA were heated to a temperature of 50 °C, and keeping the temperature conditions, the $CuSO_4$ solution was added to the hydrated ZA, applying magnetic stirring for 50 min to mix. ZACu was obtained, as a fine blue powder, which was recovered by filtration and a triple wash with deionized water to remove the remaining ions. Subsequently, it was dried at room temperature (35 °C in summer).

Step 2: Nanoparticles of Copper Sulfides in ZA ($ZACu_2S0.1$)

First, 5 g of ZACu (obtained in step 1) was dissolved in 50 ml of deionized water for 12 h for its hydration. At the same time, a solution of 150 ml of Na_2S (0.1 M) was prepared. Subsequently, the same procedure is performed as Step 1, $ZACu_2S0.1$ was obtained, as a fine green powder.

Figure 1 shows a proposed reaction mechanism for the formation of Cu_2S nanoparticles (the structure selected is named *sodalite* and could be used as a representative). Once the copper is inside ZA (step 1) the Na_2S solution is added (step 2), occurring a metathesis reaction at 50 °C. The S^{-2} ions travel through the zeolite cavities to reach and react with the copper ions of ZA, to form Cu_2S nanoparticles, in the zeolite nanoreactor. While the Na^+ ions recover their initial position in ZA and this one recovers its original structure.

Characterizations

The microstructural, morphology, size, and chemical composition of nanoparticles were analyzed by high-resolution transmission electron microscopy (HRTEM) in a JEOL JEM-2200FS + Cs equipped with a spherical aberration corrector in the condenser lens and operated at an accelerating

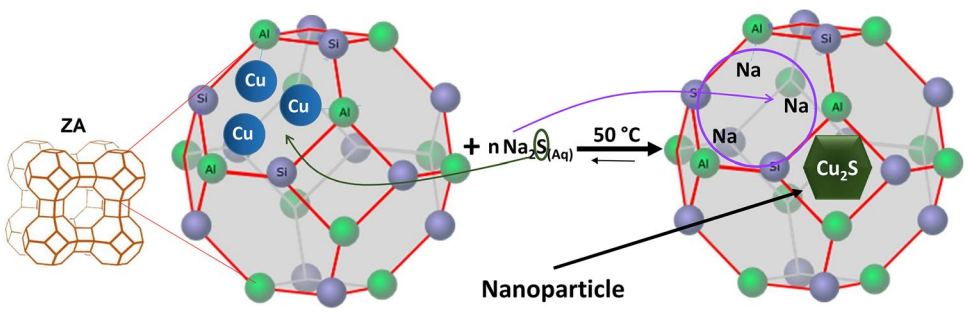

Fig. 1 Proposed reaction mechanism for Cu_2S nanoparticle formation

voltage of 200 kV. To analyze the zeolite samples by XRD, the PHI5100 BRUKER AXS D8 ADVANCE diffractometer was used. The characteristic molecular bonds of the zeolite were identified using the FT-IR spectrometer Bruker-Alpha tensor spectrophotometer. To evaluate its thermal properties, differential scanning calorimetry (DSC) SDT Q6000 was used. Absorption wavelengths of Cu_2S nanoparticles were obtained with the Perkin Elmer Lambda 19 UV–vis (powder) spectrophotometer. The vibrational energy of Cu_2S bonds was determined using a Raman spectrophotometer LABram HR Evolution, Horiba (with AFM, AIST-NT coupled).

Results and Discussion

FT-IR Analysis

Figure 2 shows the FT-IR spectra of ZA and $ZACu_2S0.1$, where peaks at 557, 667, 1000, 1657, and 3437 cm^{-1} are observed, which are characteristic of ZA [36]. Only the characteristic peaks of ZA are observed. There is no presence of Cu–O vibrations, or Copper sulfate, which have been reported as impurities in the synthesis of Cu–S nanostructures [37]. The FT-IR studies demonstrate that the molecular structure is not affected in this work that used the two steps ion-exchange method [17], and it is the first evidence of ZA, are hosting nanoparticles [38–40].

X-Ray Diffraction (XRD)

Figure 3 shows X-ray diffraction of (a) ZA and (b) $ZACu_2S0.1$. In (a) the Miller indices characteristic of ZA are observed in 2 theta range 5–37 degrees, presenting a cubic structure, lattice a = 2.461 nm, and space group Fm-3c (226) indexed by JCP2 01–073-2340. In (b) the same characteristic peaks of ZA are observed, with a slight decrease in relative peak intensity, mainly in Miller's index (220), which may be associated with the presence of Cu_2S in ZA. In addition, no

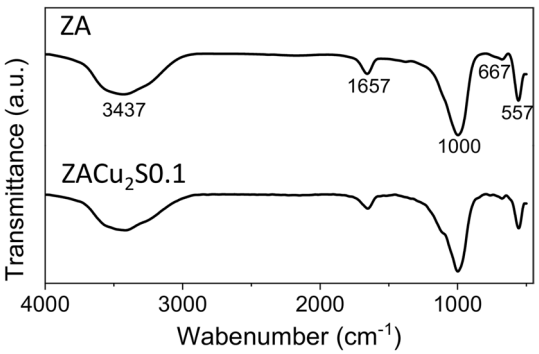

Fig. 2 FT-IR spectrum of ZA and $ZACu_2S$ 0.1

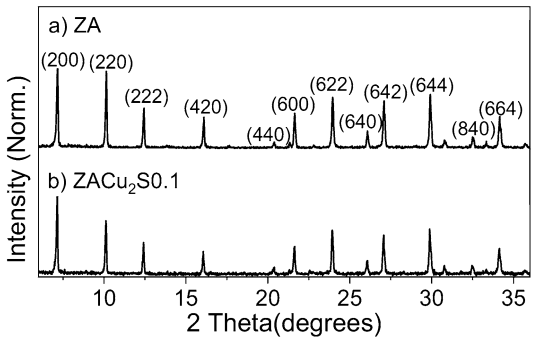

Fig. 3 X-ray diffraction of ZA and $ZACu_2S0.1$

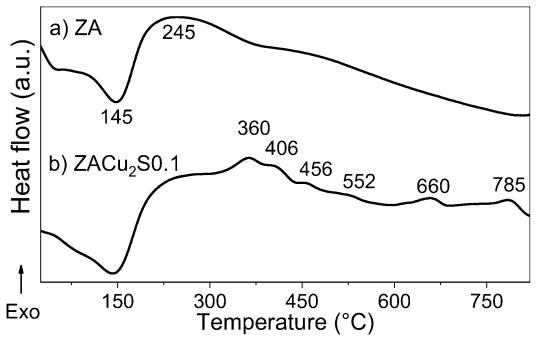

Fig. 4 DSC of **a** ZA and **b** $ZACu_2S0.1$

evidence of peaks associated with Cu_2S is observed, which may indicate that they do not satisfy the diffraction criteria [41] it is verified that the crystalline structure of ZA remains unchanged.

Differential Scanning Calorimetry (DSC)

Figure 4 shows the DSC of (a) ZA and (b) $ZACu_2S0.1$. Endothermic and exothermic signals are observed at 145 °C and 245 °C characteristics of the loss of physically and chemically housed water of ZA [42–46]. In sample (b), exothermic signals in the 360–785 °C range are observed, attributed to deformation transitions of Cu_2S, which have been reported for the formation of $Cu_{2-x}S$ nanoparticles under other synthesis methods [47, 48], demonstrating the presence of nanoparticles on the ZA matrix.

UV-Vis Spectroscopy

Figure 5 shows the optical absorption spectrum (300 to 850 nm) of (a) ZA and (b) $ZACu_2S0.1$. In (a), the spectrum is transparent with a high bandgap, by that there is no absorbance band [49]. On the other hand, in (b), shows a broad absorption band characteristic of $Cu_{2-x}S$, and most of the time, a blue-shifted peak was reported when the size

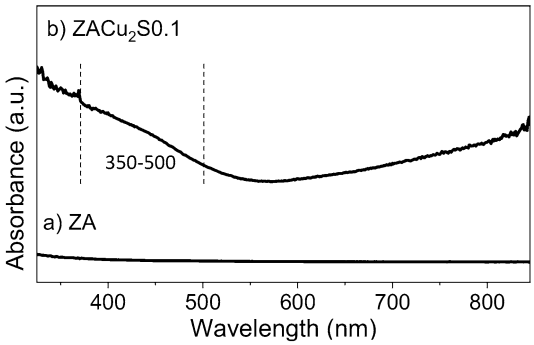

Fig. 5 UV–vis of ZA and $ZACu_2S0.1$

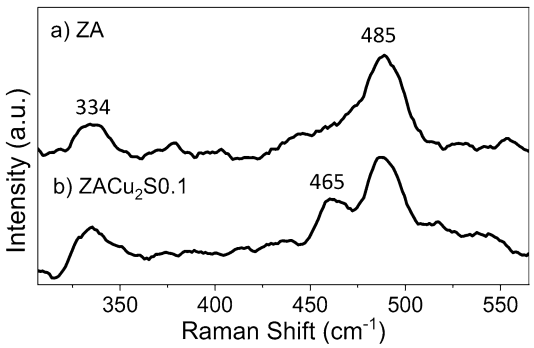

Fig. 6 Raman shift of ZA and $ZACu_2S0.1$

quantization effect is produced in the range of 5–20 nm [50]. In this case, the broadband indicates the formation of small nanoparticles [51], and the energy bandgap of 2.1 eV was calculated, characteristic of Cu_2S nanostructures [52–54]. It since is ≥ 1.2 eV for bulk copper sulphides [27, 28].

Raman Spectroscopy

Figure 6 shows the Raman spectrum of (a) ZA and (b) $ZACu_2S0.1$ in (a) Peaks at 334 and 485 cm^{-1} are observed, characteristic of ZA [55]. In (b) The peak at 465 cm^{-1} can be attributed to the Cu_2S formation, also the signal at 485 cm^{-1} has been reported for copper sulfides [56–58]. However, in this case, the zeolite peak is more intense and the interference with the Cu_2S peak can be observed.

TEM Analysis

Figure 7 shows a TEM micrograph of $ZACu_2S0.1$ which was taken in STEM mode. In this figure, a total of 170 nanoparticles were measured, with diameters in the range of 4–8 nm, with homogeneous size distribution and uniformly dispersed in the zeolite matrix.

Figure 8 shows the analysis of a TEM micrograph enlargement of $ZACu_2S0.1$, which is presented in three

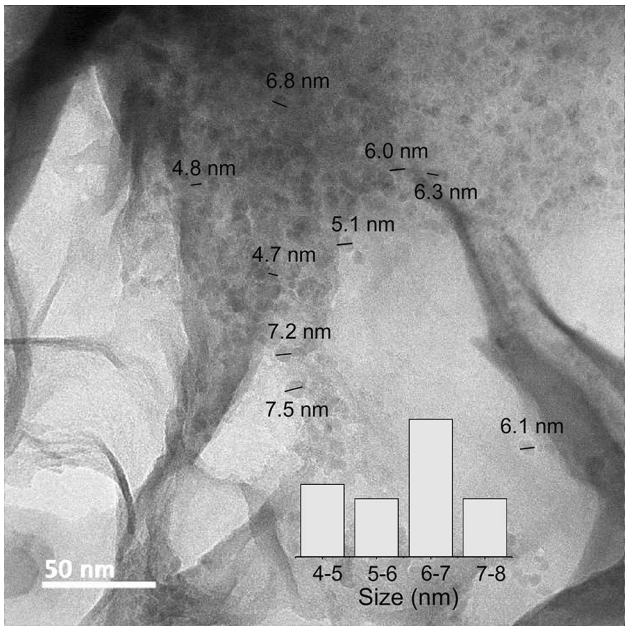

Fig. 7 TEM image taken in STEM mode of $ZACu_2S0.1$

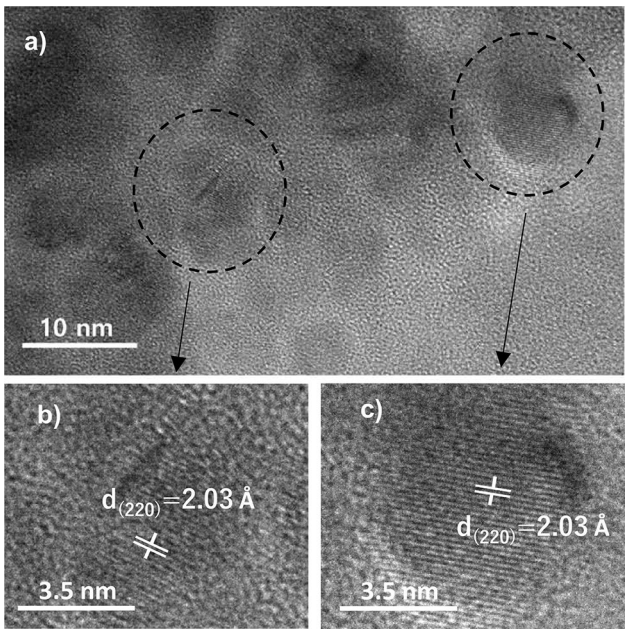

Fig. 8 **a** TEM Imagen of $Z4Cu_2S0.1$ taken in HRTEM mode; **b** and **c** are a zoom image of the square red region in **a**

parts (a–c). In (a) a micrograph taken in HRTEM mode is shown, where two nanoparticles with a size around 7 nm and semi-spherical shape are observed and were indicated with a dotted black circle. In (b) and (c) shows an enlargement of (a) in the regions dotted, where the crystalline planes with an interplanar distance of $d = 2.03$ Å is observed, corresponding to the Miller crystallographic plane (2 2 0) of Cu_2S

nanoparticles with cubic phase and *Fm-3 m* space group indexed with the JCP card number 00-012-0175.

Conclusions

The synthesis of Cu_2S ultrasmall nanoparticles in zeolite 4A nanoreactor was successfully achieved by the ion-exchange method in a two steps procedure without compromising the zeolite structure. Obtaining uniform nanoparticles with a size of 4–8 nm, homogeneously dispersed in zeolite nanoreactor and with a cubic phase.

Acknowledgements To DGIP of the Universidad Autónoma de Sinaloa (UAS), for the financial support through the PROFAPI2015/100 Project, to the Consejo Nacional de Ciencia y Tecnología (CONACYT) for their support of scholarships No. 775836, and to the Centro de Investigación en Materiales Avanzados, S.C. (CIMAV), for its support in infrastructure and equipment.

Declarations

Conflict of Interest The authors have no relevant financial or non-financial interests to disclose. The authors have no conflicts of interest to declare that are relevant to the content of this article.

References

1. L. P. Wang, A. Titov, R. McGibbon, et al. (2014). Discovering chemistry with an ab initio nanoreactor. *Nat Chem* **6**, 1044–1048. https://doi.org/10.1038/nchem.2099.
2. M. T. De Martino, L. K. E. A. Abdelmohsen, F. P. J. T. Rutjes, and J. C. M. Van Hest (2018). Nanoreactors for green catalysis. *Beilstein J Org Chem* **14**, 716–733. https://doi.org/10.3762/bjoc.14.61.
3. J. H. Lee, W. Bonte, S. Corthals, et al. (2019). Zeolite nanoreactor for investigating sintering effects of cobalt-catalyzed Fischer-Tropsch synthesis. *Ind Eng Chem Res* **58**, 5140–5145. https://doi.org/10.1021/acs.iecr.8b05755.
4. J. Li, A. Corma, and J. Yu (2015). Synthesis of new zeolite structures. *Chem Soc Rev* **44**, 7112–7127. https://doi.org/10.1039/c5cs00023h.
5. S. E. Lehman and S. C. Larsen (2014). Zeolite and mesoporous silica nanomaterials: greener syntheses, environmental applications and biological toxicity. *Environ Sci Nano* **1**, 200–213. https://doi.org/10.1039/c4en00031e.
6. S. Sugiyama, S. Yamamoto, O. Matsuoka, et al. (1999). AFM observation of double 4-rings on zeolite LTA crystals surface. *Microporous Mesoporous Mater* **28**, 1–7. https://doi.org/10.1016/S1387-1811(98)00271-6.
7. C. Chuapradit, L. R. Wannatong, D. Chotpattananont, et al. (2005). Polyaniline/zeolite LTA composites and electrical conductivity response towards CO. *Polymer (Guildf)* **46**, 947–953. https://doi.org/10.1016/j.polymer.2004.11.101.
8. Z. Xue, J. Ma, W. Hao, et al. (2012). Synthesis and characterization of ordered mesoporous zeolite LTA with high ion exchange ability. *J Mater Chem* **22**, 2532–2538. https://doi.org/10.1039/c1jm14740d.
9. Y. C. Feng, Y. Meng, F. X. Li, et al. (2013). Synthesis of mesoporous LTA zeolites with large BET areas. *J Porous Mater* **20**, 465–471. https://doi.org/10.1007/s10934-012-9617-7.
10. Y. Chai, W. Shang, W. Li, et al. (2019). Noble metal particles confined in zeolites: synthesis, characterization, and applications. *Adv Sci* **6**, 1900299. https://doi.org/10.1002/advs.201900299.
11. E. Coutino-Gonzalez, M. Roeffaers, and J. Hofkens, *Highly luminescent metal clusters confined in zeolites*. (Springer, Cham, 2020), pp. 75–103.
12. P. Cao, L. Lin, H. Qi, et al. (2021). Zeolite-encapsulated Cu nanoparticles for the selective hydrogenation of furfural to furfuryl alcohol. *ACS Catal* **11**, 10246–10256. https://doi.org/10.1021/acscatal.1c02658.
13. L. Du, M. Yuan, H. Wei, et al. (2019). Interconnected Pd nanoparticles supported on zeolite-AFI for hydrogen detection under ultralow temperature. *ACS Appl Mater Interfaces* **11**, 36847–36853. https://doi.org/10.1021/acsami.9b12272.
14. D. Farrusseng and A. Tuel (2016). Perspectives on zeolite-encapsulated metal nanoparticles and their applications in catalysis. *New J Chem* **40**, 3933–3949. https://doi.org/10.1039/c5nj02608c.
15. L. Wang, S. Xu, S. He, and F. S. Xiao (2018). Rational construction of metal nanoparticles fixed in zeolite crystals as highly efficient heterogeneous catalysts. *Nano Today* **20**, 74–83. https://doi.org/10.1016/j.nantod.2018.04.004.
16. J. Zhang, X. Bu, P. Feng, and T. Wu (2020). Metal chalcogenide supertetrahedral clusters: synthetic control over assembly, dispersibility, and their functional applications. *ACC Chem Res* **53**, 2261–2272. https://doi.org/10.1021/acs.accounts.0c00381.
17. D. Hu, X. Wang, H. Yang, et al. (2018). Host-guest electrocatalyst with cage-confined cuprous sulfide nanoparticles in etched chalcogenide semiconductor zeolite for highly efficient oxygen reduction reaction. *Electrochim Acta* **282**, 877–885. https://doi.org/10.1016/j.electacta.2018.06.106.
18. A. D. Terna, E. E. Elemike, J. I. Mbonu, et al. (2021). The future of semiconductors nanoparticles: Synthesis, properties and applications. *Mater Sci Eng B Solid-State Mater Adv Technol* **272**, 115363. https://doi.org/10.1016/j.mseb.2021.115363.
19. M. S. Sadjadi, A. Pourahmad, S. Sohrabnezhad, and K. Zare (2007). Formation of NiS and CoS semiconductor nanoparticles inside mordenite-type zeolite. *Mater Lett* **61**, 2923–2926. https://doi.org/10.1016/j.matlet.2006.10.067.
20. S. Sahoo, R. Mondal, D. J. Late, and C. S. Rout (2017). Electrodeposited Nickel Cobalt Manganese based mixed sulfide nanosheets for high performance supercapacitor application. *Microporous Mesoporous Mater* **244**, 101–108. https://doi.org/10.1016/j.micromeso.2017.02.043.
21. F. Márquez and V. Fornés (1999). Synthesis and characterisation of Ga2S3 semiconductor included in zeolite Y. *Solid State Commun* **112**, 17–20. https://doi.org/10.1016/S0038-1098(99)00295-1.
22. R. Ochoa-Landín, M. Flores-Acosta, R. Ramírez-Bon, et al. (2003). Characterization of Cds clusters in zeolite-A grown in alkaline solution. *J Phys Chem Solids* **64**, 2245–2251. https://doi.org/10.1016/S0022-3697(03)00243-9.
23. E. Caponetti, L. Pedone, M. L. Saladino, et al. (2010). MCM-41-CdS nanoparticle composite material: Preparation and characterization. *Microporous Mesoporous Mater* **128**, 101–107. https://doi.org/10.1016/j.micromeso.2009.08.010.
24. G. Guan, T. Kida, K. Kusakabe, et al. (2005). Photocatalytic activity of CdS nanoparticles incorporated in titanium silicate molecular sieves of ETS-4 and ETS-10. *Appl Catal A Gen* **295**, 71–78. https://doi.org/10.1016/j.apcata.2005.08.010.
25. H. Peng, S. M. Liu, L. Ma, et al. (2001). Growing process of CdS nanoclusters in zeolite Y studied by positron annihilation. *J Cryst Growth* **224**, 274–279. https://doi.org/10.1016/S0022-0248(01)00972-1.

26. Y. Liu, M. Liu, and M. T. Swihart (2017). Reversible crystal phase interconversion between covellite CuS and high chalcocite Cu2S nanocrystals. *Chem Mater* **29**, 4783–4791. https://doi.org/10.1021/acs.chemmater.7b00579.
27. Y. Lou, X. Chen, A. C. Samia, and C. Burda (2003). Femtosecond spectroscopic investigation of the carrier lifetimes in digenite quantum dots and discrimination of the electron and hole dynamics via ultrafast interfacial electron transfer. *J Phys Chem B* **107**, 12431–12437. https://doi.org/10.1021/jp035618k.
28. J. Kolny-Olesiak (2014). Synthesis of copper sulphide-based hybrid nanostructures and their application in shape control of colloidal semiconductor nanocrystals. *CrystEngComm* **16**, 9381–9390. https://doi.org/10.1039/c4ce00674g.
29. A. L. Soares, E. C. Dos Santos, A. Morales-García, et al. (2017). Two-dimensional crystal CuS-electronic and structural properties. *2D Mater* **4**, 015041. https://doi.org/10.1088/2053-1583/aa516e.
30. R. Marshall and S. S. Mitra (1965). Optical properties of cuprous sulfide. *J Appl Phys* **36**, 3882–3883. https://doi.org/10.1063/1.1713966.
31. Z. Wang, X. Tang, X. Wang, et al. (2016). Near-infrared light-induced dissociation of zeolitic imidazole framework-8 (ZIF-8) with encapsulated CuS nanoparticles and their application as a therapeutic nanoplatform. *Chem Commun* **52**, 12210–12213. https://doi.org/10.1039/c6cc06616j.
32. E. I. Torres-Flores, N. S. Flores-López, C. E. Martínez-Núñez, et al. (2021). Silver nanoparticles in natural zeolites incorporated into commercial coating: antibacterial study. *Appl Phys A Mater Sci Process* **127**, 1–11. https://doi.org/10.1007/s00339-020-04227-5.
33. H. J. Cho, D. Kim, J. Li, et al. (2018). Zeolite-encapsulated Pt nanoparticles for tandem catalysis. *J Am Chem Soc* **140**, 13514–13520. https://doi.org/10.1021/jacs.8b09568.
34. J. Zhang, L. Wang, B. Zhang, et al. (2018). Sinter-resistant metal nanoparticle catalysts achieved by immobilization within zeolite crystals via seed-directed growth. *Nat Catal* **1**, 540–546. https://doi.org/10.1038/s41929-018-0098-1.
35. J. Flores-Valenzuela, M. Cortez-Valadez, R. Ramírez-Bon, et al. (2015). Optical and vibrational properties of PbSe nanoparticles synthesized in clinoptilolite. *Phys E Low-Dimensional Syst Nanostructures* **72**, 1–6. https://doi.org/10.1016/j.physe.2015.04.012.
36. R. Kefirov, A. Penkova, K. Hadjiivanov, et al. (2008). Stabilization of Cu+ ions in BEA zeolite: study by FTIR spectroscopy of adsorbed CO and TPR. *Microporous Mesoporous Mater* **116**, 180–187. https://doi.org/10.1016/j.micromeso.2008.03.032.
37. A. Kusior, P. Jelen, J. Mazurkow, et al. (2019). Synthesis of anisotropic Cu2−xS-based nanostructures by thermal oxidation. *J Therm Anal Calorim* **138**, 4321–4329. https://doi.org/10.1007/s10973-019-08622-w.
38. S. Şen, B. Bardakçi, A. G. Yavuz, and A. U. Gök (2008). Polyfuran/zeolite LTA composites and adsorption properties. *Eur Polym J* **44**, 2708–2717. https://doi.org/10.1016/j.eurpolymj.2008.05.018.
39. T. Montanari and G. Busca (2008). On the mechanism of adsorption and separation of CO2 on LTA zeolites: an IR investigation. *Vib Spectrosc* **46**, 45–51. https://doi.org/10.1016/j.vibspec.2007.09.001.
40. W. Mozgawa, M. Król, and K. Barczyk (2011). FT-IR studies of zeolites from different structural groups. *Chemik* **65**, 671–674.
41. B. E. Warren (1941). X-ray diffraction methods. *J Appl Phys* **12**, 375–383. https://doi.org/10.1063/1.1712915.
42. M. K. Doula (2007). Synthesis of a clinoptilolite-Fe system with high Cu sorption capacity. *Chemosphere* **67**, 731–740. https://doi.org/10.1016/j.chemosphere.2006.10.072.
43. R. M. Mohamed and M. M. Mohamed (2008). Copper (II) phthalocyanines immobilized on alumina and encapsulated inside zeolite-X and their applications in photocatalytic degradation of cyanide: a comparative study. *Appl Catal A Gen* **340**, 16–24. https://doi.org/10.1016/j.apcata.2008.01.029.
44. A. Nezamzadeh-Ejhieh and S. Hushmandrad (2010). Solar photodecolorization of methylene blue by CuO/X zeolite as a heterogeneous catalyst. *Appl Catal A Gen* **388**, 149–159. https://doi.org/10.1016/j.apcata.2010.08.042.
45. R. V. Siriwardane, M. S. Shen, E. P. Fisher, and J. Losch (2005). Adsorption of CO2 on zeolites at moderate temperatures. *Energy Fuels* **19**, 1153–1159. https://doi.org/10.1021/ef040059h.
46. A. Aho, N. Kumar, K. Eränen, et al. (2008). Catalytic pyrolysis of woody biomass in a fluidized bed reactor: influence of the zeolite structure. *Fuel* **87**, 2493–2501. https://doi.org/10.1016/j.fuel.2008.02.015.
47. M. Nafees, M. Ikram, and S. Ali (2015). Thermal behavior and decomposition of copper sulfide nanomaterial synthesized by aqueous sol method. *Dig J Nanomater Biostructures* **10**, 635–641.
48. M. Nafees, S. Ali, S. Idrees, et al. (2013). A simple microwave assists aqueous route to synthesis CuS nanoparticles and further aggregation to spherical shape. *Appl Nanosci* **3**, 119–124. https://doi.org/10.1007/s13204-012-0113-9.
49. T. Jüstel, D. U. Wiechert, C. Lau, et al. (2001). Optically functional zeolites: evaluation of UV and VUV stimulated photoluminescence properties of Ce3+- and Tb3+-doped zeolite X. *Adv Funtional Mater* **11**, 105–110. https://doi.org/10.1002/1616-3028(200104)11:2%3c105::AID-ADFM105%3e3.0.CO;2-J.
50. Y. Zhao, H. Pan, Y. Lou, et al. (2009). Plasmonic Cu 2-xS nanocrystals: optical and structural properties of copper-deficient copper(I) sulfides. *J Am Chem Soc* **131**, 4253–4261. https://doi.org/10.1021/ja805655b.
51. K. D. Sattler, *Handbook of nanophysics* (CRC Press, 2010).
52. C. Wu, Shi J. Bin, C. J. Chen, et al. (2008). Synthesis and optical properties of CuS nanowires fabricated by electrodeposition with anodic alumina membrane. *Mater Lett* **62**, 1074–1077. https://doi.org/10.1016/j.matlet.2007.07.046.
53. Z. Liu, D. Xu, J. Liang, et al. (2005). Growth of Cu2S ultrathin nanowires in a binary surfactant solvent. *J Phys Chem B* **109**, 10699–10704. https://doi.org/10.1021/jp050332w.
54. S. T. Connor, C. M. Hsu, B. D. Weil, et al. (2009). Phase transformation of biphasic Cu 2S-CuInS 2 to monophasic CuInS 2 nanorods. *J Am Chem Soc* **131**, 4962–4966. https://doi.org/10.1021/ja809901u.
55. Y. Yu, G. Xiong, C. Li, and F. S. Xiao (2001). Characterization of aluminosilicate zeolites by UV Raman spectroscopy. *Microporous Mesoporous Mater* **46**, 23–34. https://doi.org/10.1016/S1387-1811(01)00271-2.
56. L. Zhang, J. Fang, M. Li, et al. (2014). Annealing effects on CuInS2 thin films grown on glass substrates by using pulsed laser deposition. *J Korean Phys Soc* **64**, 410–414. https://doi.org/10.3938/jkps.64.410.
57. A. G. Milekhin, N. A. Yeryukov, L. L. Sveshnikova, et al. (2015). Combination of surface- and interference-enhanced Raman scattering by CuS nanocrystals on nanopatterned Au structures. *Beilstein J Nanotechnol* **6**, 749–754. https://doi.org/10.3762/bjnano.6.77.
58. S. Ren, L. Li, Z. Liu, et al. (2012). The light absorption properties of Cu 2S nanowire arrays. *Adv Mater Res*. https://doi.org/10.4028/www.scientific.net/AMR.528.272.